*29th EPS Conference on Plasma Phys. and Contr. Fusion Montreux, 17-21 June 2002 ECA Vol. **26B**, P-1.091 (2002)*

Quantitative Tests of ELMs as Intermediate *n* Peeling-Ballooning Modes

L.L. Lao,[1] P.B. Snyder,[1] A.W. Leonard,[1] T.H. Osborne,[1] T.W. Petrie,[1] J.R. Ferron,[1] R.J. Groebner,[1] L.D. Horton,[2] Y. Kamada,[3] M. Murakami,[4] T. Oikawa,[3] L.D. Pearlstein,[5] S. Saarelma,[6] H.E. St. John,[1] D.M. Thomas,[1] A.D. Turnbull,[1] H.R. Wilson[7]

[1]*General Atomics, P.O. Box 85608, San Diego, California, 92186-5608 USA*
[2]*Max Planck Institute of Plasma Physics, Garching, Germany*
[3]*Japan Atomic Energy Research Institute, Naka-machi, Naka-gun, Ibaraki-ken, Japan*
[4]*Oak Ridge National Laboratory, Oak Ridge, Tennessee, 37831 USA*
[5]*Lawrence Livermore National Laboratory, Livermore, California, 94551 USA*
[6]*Helsinki University of Technology, Finland*
[7]*Euratom/UKAEA Fusion Association, Culham Science Centre, Abington, UK*

I. INTRODUCTION

Two of the major issues crucial for the design of the next generation tokamak burning plasma devices are the predictability of the edge pedestal height and control of the divertor heat load in H–mode configurations. Both of these are strongly impacted by edge localized modes (ELMs) and their size. A working model for ELMs is that they are intermediate toroidal mode number, $n \sim 5$–30, peeling-ballooning modes driven by the large edge pedestal pressure gradient P' and the associated large edge bootstrap current density J_{BS} [1–3]. The interplay between P' and J_{BS} as a discharge evolves can excite peeling-ballooning modes over a wide spectrum of n. The pedestal current density plays a dual role by stabilizing the high n ballooning modes via opening access to second stability but providing free energy to drive the intermediate n peeling modes. This makes a systematic evaluation of this model particularly challenging.

This paper describes recent quantitative tests of this model using experimental data from the DIII–D and the JT-60U tokamaks. These tests are made possible by recent improvements to the ELITE MHD stability code [3,4], which allow an efficient evaluation of the unstable peeling-ballooning modes, as well as by improvements to other diagnostic and analysis techniques. Some of the key testable features of this model are:

1. ELMs are triggered when the growth rates of intermediate n MHD modes become significantly large;
2. ELM sizes are related to the radial widths of the unstable modes;
3. The unstable modes have a strong ballooning character localized in the outboard bad curvature region;
4. At high collisionality, ELM size generally becomes smaller because J_{BS} is reduced.

II. ELM SIZE

In this model, the ELM size is assumed to be related to the radial width of the unstable MHD modes. This feature is consistent with many experimental observations in DIII–D and JT-60U discharges. The calculated growth rate attains a significant value just before an ELM occurs. The observed change in electron temperature $\Delta T_e/T_e$ from statistical analysis of DIII–D Thomson data is consistent with the calculated radial width of the most unstable peeling-ballooning mode [3]. This is illustrated in Fig. 1, where the relative change in $\Delta T_e/T_e$ immediately after a giant ELM for a DIII–D discharge is compared against the radial width of the $n = 10$ unstable eigenmode. The unstable peeling-ballooning modes are computed using the ELITE code based on experimental equilibria reconstructed from kinetic profiles and MSE data. The $n = 10$ mode is chosen for the comparison since it has the largest growth rate

normalized to the diamagnetic frequency, γ/ω_*. The change in $\Delta T_e/T_e$ is estimated by ordering the measured T_e profiles in time with respect to the ELMs over many ELM cycles and extrapolating the results to the time immediately after an ELM crash. Also shown in the inset of Fig. 1 is the 2-D contour of the MHD radial displacement. The perturbations are strongly pressure-driven and have a dominant ballooning character localized in the outboard bad curvature region. This is further discussed in Section III.

The predicted radial widths of the unstable peeling-ballooning modes are also consistent with the JT-60U giant and grassy ELM experimental results. The predicted unstable modes in the JT-60U grassy ELM discharges using ELITE based on experimental equilibria have narrower radial widths than those predicted for discharges with giant type I ELMs [5].

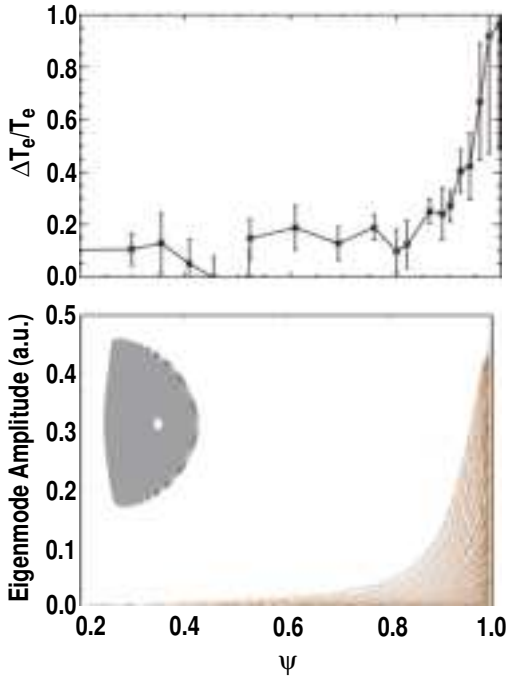

Fig. 1. Comparison of the radial profile of $\Delta T_e/T_e$ right after a giant ELM for DIII–D discharge 97887 against the radial structure of the unstable n = 10 peeling-ballooning mode computed using ELITE. A contour plot of the radial displacement of the unstable mode is shown in the inset.

III. BALLOONING CHARACTER

The unstable MHD modes are driven by the edge pedestal P′ and the associated edge J_{BS}. Bad curvature plays a strong role in the instability. Thus, the predicted poloidal structure of the unstable eigenmodes have a strong ballooning character localized in the outboard bad curvature region, as illustrated in the inset of Fig. 1. This predicted feature is consistent with the experimental results from the DIII–D divertor balance experiments [6]. ELM-generated particle fluxes to the upper inner strike point are observed in the upper-single-null divertor discharges, but are absent in the lower single-null and the double-null discharge when they are topologically disconnected from the outer midplane. This is illustrated in Fig. 2, where the particle fluxes at various poloidal locations around the divertor from Langmuir probe measurements for a lower-single-null discharge, a double-null discharge, and an upper-single-null discharge are compared. The 2-D contours of the radial displacements computed using ELITE, based on experimentally reconstructed equilibria from these three discharges, are shown in Fig. 2(b). The perturbations are localized in the outboard bad curvature regions due to the strong ballooning character, consistent with the measurements of the ELM-generated particle fluxes in these discharges.

This predicted ballooning character is also consistent with the Mirnov oscillations sometimes observed in DIII–D discharges prior to a giant type I ELM. These magnetic oscillations rotate in the electron diamagnetic direction, which is consistent with localization of these modes in the plasma edge region [7]. The Mirnov oscillations also have a strong ballooning character localized poloidally in the outboard bad curvature region. Localized reflectometer measurements at the outboard mid-plane indicate that the perturbations start in the high pedestal pressure gradient region and propagate outwards into the scrape-off layer [1].

IV. COLLISIONALITY

Both the edge J_{BS} as well as the edge pedestal P′ drive the MHD modes. As the edge density and hence the edge collisionality is increased, the ELM size is generally predicted to

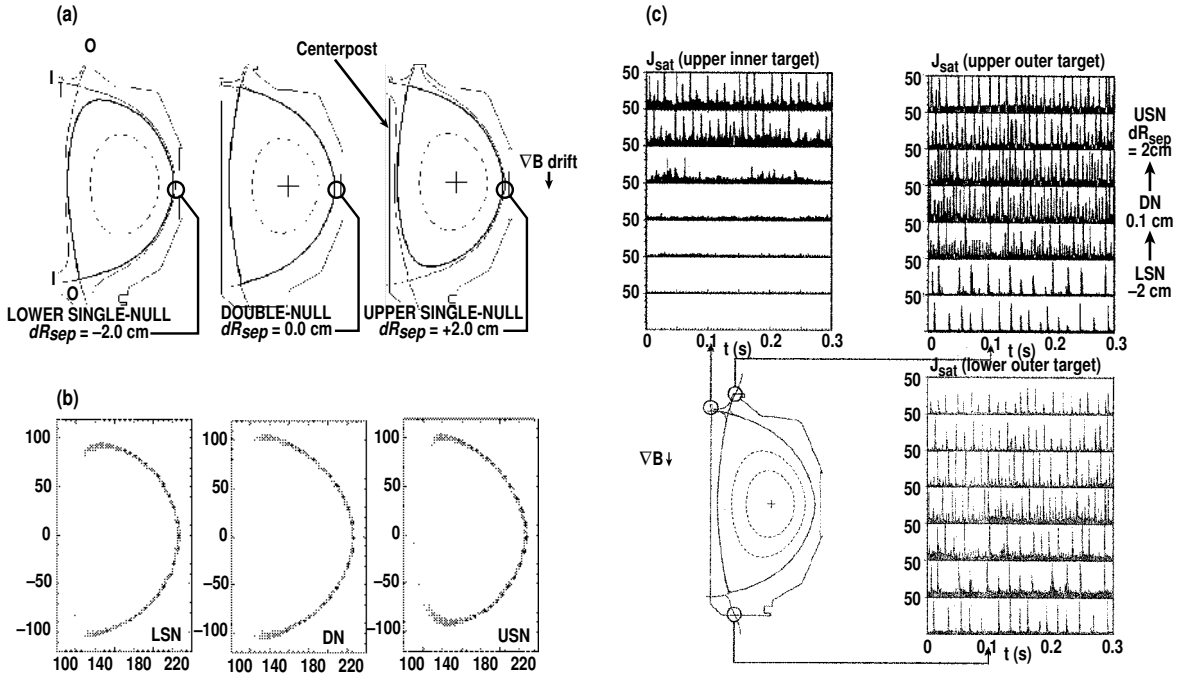

Fig. 2. (a) The lower-single-null (LSN), the double-null (DN), and the upper-single-null (USN) divertor configurations used in the DIII–D divertor balance experiments. dR_{sep} denotes the radial difference in the upper divertor separatrix flux surface and the lower divertor separatrix flux surface at the outer mid-plane. (b) Contours of the radial displacement of the unstable n = 25 peeling-ballooning modes showing the localization of the perturbations in the outboad bad curvature regions. (c) ELM-generated particle fluxes from Langmuir probes at various poloidal locations around the divertor showing the absence of ELM-generated particle flux in the double-null and the lower-single-null divertor discharges.

become smaller since J_{BS} is reduced. This is consistent with the experimental results from the DIII–D gas puff experiments, as illustrated in Figs. 3 and 4. In Fig. 3, the ELM energy losses determined from equilibrium recon-structions using fast magnetic measurements for two DIII–D discharges with the edge Greenward density parameter n_e/n_{GW} = 0.52 and 0.74 are compared. The ELM energy loss is substantially reduced in the higher density discharge. The radial structures of the unstable eigenmodes computed using ELITE based on experimental equilibria are compared in Fig. 4. In these equilibria, the edge J is constrained using a bootstrap current model. As shown in Fig. 4, the unstable MHD mode for the smaller ELM, higher density discharge has a narrower radial width than the larger ELM, lower density discharge. The unstable mode in the higher density case has n = 25 and the lower density case has n = 10. The increase in edge J_{BS} in the lower density case stabilizes the high n modes, but destabilizes the lower n instabilities. This is illustrated in Fig. 5, where the high n ballooning stability diagrams for these two cases are compared. The lower density case has second ballooning stability access in the plasma edge, whereas the higher density case does not. The edge second ballooning stability access in the lower density discharge is consistent with the wider edge pressure pedestal observed in this discharge.

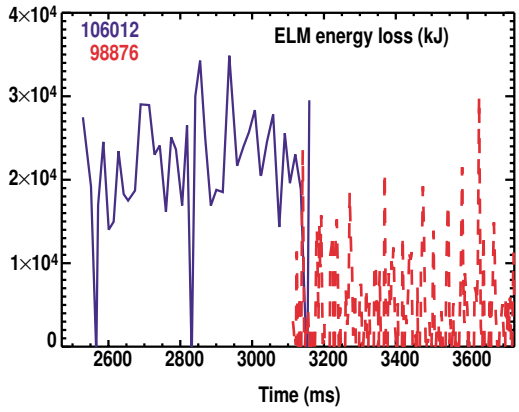

Fig. 3. Comparison of ELM energy loss for 2 DIII–D discharges with edge n_e/n_{GW} = 0.52 (solid curve) and n_e/n_{GW} = 0.74 (dashed curve).

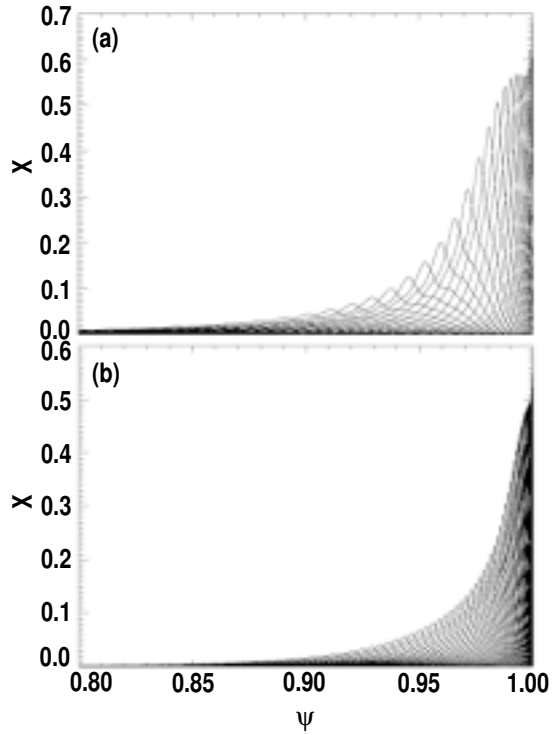

Fig. 4. Comparison of the radial structure of the unstable eigenmodes for 2 DIII–D discharges shown in Fig. 3. (a) edge n_e/n_{GW} = 0.52 and n = 10 and (b) n_e/n_{GW} = 0.74 and n = 25.

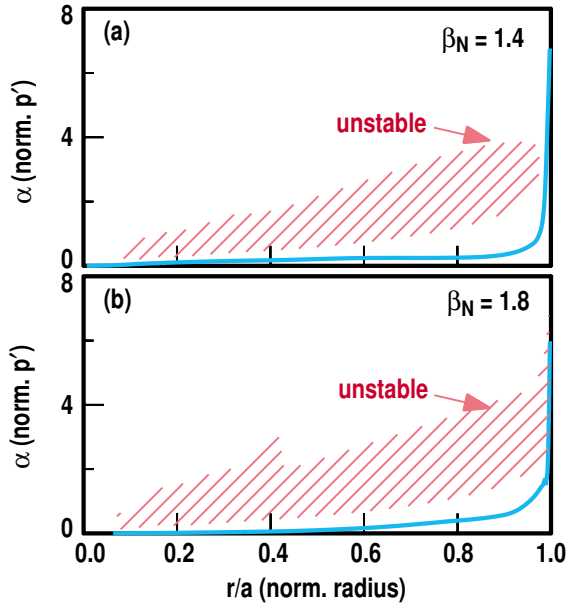

Fig. 5. Comparison of the high n ballooning stability boundary for 2 DIII–D discharges shown in Fig. 3. (a) edge n_e/n_{GW} = 0.52 and (b) edge n_e/n_{GW} = 0.74.

V. SUMMARY

The predicted features of the working model of ELMs as intermediate n ~ 5–30 peeling-ballooning modes are consistent with many ELM observations in DIII–D and JT-60U discharges. ELMs are triggered when the growth rates of the intermediate n MHD modes become sufficiently large. The unstable modes have a strong ballooning character localized in the outboard bad curvature region. The ELM size is related to the radial width of the unstable MHD modes.

ACKNOWLEDGMENT

Work supported by the U.S. Department of Energy under Contracts DE-AC03-99ER54463, DE-AC05-00OR22725. W-7405-ENG-48, Grant DE-FG03-99ER54541.

REFERENCES

[1] Lao, L.L., J.R. Ferron, J., Miller, R.L., *et al*., Nucl. Fusion **39**, 1785 (1999).
[2] Ferron, J.R., Chu, M.S., G.L. Jackson, Lao, L.L., *et al*., Phys. Plasmas **7**, 1976 (2000).
[3] Snyder, P.B., Wilson, H.R., Ferron, J.R., Lao, L.L., *et al*., Phys. Fluids **9**, 2037 (2002).
[4] Wilson, H.R., Snyder, P.B., et al., Phys. Fluids **9**, 1277 (2002).
[5] Lao, L.L., Kamada, Y., Oikawa, T., *et al*., Nucl. Fusion **41**, 295 (2001).
[6] Petrie, T.W., *et al*., GA-A23895, 2002, submitted to Phys. Rev. Lett.
[7] Strait, E.J., *et al*., Phys. Plasmas **4**, 1783 (1997).